Korean J. Chem. Eng., 37(3), 411-422 (2020)
DOI: 10.1007/s11814-019-0453-1

pISSN: 0256-1115
eISSN: 1975-7220

Experimental study and artificial intelligence modeling of liquid-liquid mass transfer in multiple-ring microchannels

Fardin Hosseini and Masoud Rahimi†

CFD Research Center, Chemical Engineering Department, Razi University, Kermanshah, Iran

(*Received 22 September 2019 • accepted 4 December 2019*)

Abstract−This paper reports the results of using multiple-ring microchannels for enhancing liquid-liquid extraction performance. The effects of geometrical parameters including ring and distance characteristics on the extraction efficiency were studied. The mass transfer performance was analyzed using Water+Alizarin Red S+1-octanol system. By change in geometrical parameters, the extraction efficiency of multiple-ring microchannels improved up to 62.9% compared with that of the plain one. The performance ratio is defined based on two contrary effects of friction factor and extraction efficiency for evaluating the extraction performance. A performance ratio of 1.5 was achieved that confirmed the advantage of using this type of microfluidic extraction system. Artificial neural network and adaptive neuro-fuzzy inference system were utilized to evaluate the performance ratio of the multiple-ring microchannels. The mean relative error values of the testing data were 0.397% and 0.888% for the neural network and the neuro-fuzzy system, respectively. The estimation accuracy for both models is appropriate, but the precision of the neural network id higher than that of the neuro-fuzzy system. The genetic algorithm approach was employed to develop a new empirical correlation for predicting the performance ratio with a mean relative error of 1.558%.

Keywords: Multiple-ring Microchannels, Liquid-liquid Mass Transfer, ANN, ANFIS, Genetic Algorithm

INTRODUCTION

Microfluidic technology is an advanced technology that offers advantages of fluid flow in micro-structure systems. Microfluidic systems with at least one dimension on the order of microns have gained widespread attention in a wide range of applications. Microfluidic systems provide some advantages, such as lower reagent consumption, faster mixing, higher throughput, and cheaper fabrication cost compared with large-scale devices [1]. Common applications of the microfluidic systems include chemical synthesis, separation processes, sample preparation, and biological engineering [2,3]. Microchannels are important components of the microfluidic systems. A well-designed microchannel can reduce diffusion length and increase the surface-to-volume ratio of a lab-on-a-chip system [4-7]. These features lead to a higher mass transfer rate in various geometries of microchannels compared with large-scale mass transfer systems [8].

Liquid-liquid extraction is widely used as a separation process in various fields such as analytical chemistry, environmental sciences, chemical engineering, and biology [8]. Microchannels are very efficient for liquid-liquid extraction. The extraction performance of different types of microchannels has been investigated by many researchers [8,9]. Zhang et al. [10] performed the liquid-liquid extraction of Nd (III) in a narrow micromixer and investigated the effects of operating parameters on the extraction efficiency. Extraction equilibrium was achieved with a residence time of 1.5 s in a microchannel without mechanical mixing. Kaewchad et al. [11] used a T-type microchannel for liquid-liquid extraction of toluene from heptane. Excellent extraction performance was obtained by the microtube extractor compared with other systems.

Alizarin Red S is a water-soluble dye that is widely utilized in textile industries. It is well known that the treatment of wastewaters containing durable dyes is very difficult because molecules of these chemicals are resistant to traditional aerobic treatment. Solvent extraction using microfluidic systems is an efficient process because of its high efficiency.

In most cases of micromixers, because of small dimensions of the channel, Reynolds number values are low and the fluid flow regime is laminar. Due to the lack of turbulence in the laminar flow, the mixing is mainly achieved by molecular diffusion. Different shapes of the micromixers provide various diffusion paths and contact areas between samples. Therefore, the geometry of the micromixers is a significant parameter to improve fluid mixing in these devices. The mixing performance in various geometries of the microchannels has been investigated by many researchers [12]. Hossain et al. [13] investigated the mixing performance and flow fields of water-toluene system in various micromixers such as zigzag, square-wave, and curved by a numerical study. Shah et al. [14] analyzed the mixing efficiency in three types of split and recombination micromixers using experimental work and numerical simulation. The pressure drop and mixing index of each micromixer were evaluated. The results of this research showed that the mixing index in the proposed micromixers improves compared with the straight mixer.

Artificial neural network (ANN) is an efficient technique for solving complex non-linear functions in different fields with a significant reduction in time and cost. The ANN has some features

†To whom correspondence should be addressed.
E-mail: masoudrahimi@yahoo.com, m.rahimi@razi.ac.ir

such as high processing rate, wide capacity, and availability of the multiple training algorithms. This technique has been used for modeling different engineering problems [15,16]. Adaptive neuro-fuzzy inference system (ANFIS) is created by combining the neural network and the fuzzy inference system. In fact, the neural network with learning ability can specify the fuzzy inference system parameters. Krishna et al. [17] employed the ANFIS and ANN methods for modeling the fluidized bed hydrodynamics. The results of error analysis indicated that the precision of the ANFIS model is higher compared to the ANN model. Lashkaripour et al. [18] utilized the ANFIS approach for predicting the droplet size in a micromixer. The input parameters were micromixer geometry, fluid flow, and fluid properties. The results showed an acceptable precision for the ANFIS model.

In this research, multiple-ring microchannels were used to intensify the liquid-liquid extraction. To the best of our knowledge, the effect of this geometry of microchannels on the mass transfer characteristics has not been investigated. Seven multiple-ring microchannels with different geometries were used. The extraction of Alizarin Red S from water using the organic phase was performed in the microchannels at different Reynolds numbers. Although the multiple-ring microchannels have a positive effect on the mass transfer performance, they lead to a higher pressure drop compared to straight channels. Therefore, the performance ratio criterion was used for evaluating the studied microchannels. Proposing trustworthy estimation models is required for finding more efficient geometrical parameters. In this regard, ANN and ANFIS models were developed to predict the performance ratio of multiple-ring microchannels. Modeling the performance ratio with ANN and ANFIS approaches has not been reported in the literature. The input parameters of the models were Reynolds number, ring characteristic, and distance characteristic. Moreover, a novel empirical equation was proposed to estimate the performance ratio of the studied microchannels and the genetic algorithm technique was used to find the equation constants.

EXPERIMENTAL

1. Material

The materials in the present liquid-liquid extraction process included Alizarin Red S, 1-octanol, and Aliquat 336. Alizarin Red S as the transferable component from the aqueous solution into the organic solution was purchased from Sigma-Aldrich. The chemical formula of Alizarin Red S is $C_{14}H_7NaO_7S$. 1-octanol as the diluent in the organic phase was supplied from Merck. Aliquat 336 with the chemical formula of $C_{25}H_{54}ClN$ was used as the extractant in the organic phase and it was provided by Sigma-Aldrich.

2. Apparatus

A schematic layout of the experimental setup is demonstrated in Fig. 1. Liquid-liquid extraction was performed in the multiple-ring microchannels to determine the mass transfer performance. The multiple-ring microchannels were made by copper microtubes with an inner diameter of 0.8 mm. The rings in each microchannel were made consistently so that their diameter was same. The total length of the microchannels was fixed at 50 cm to fix the mixing channel volume and accordingly fluid residence time. This was performed to make the extraction efficiency independent of the residence time when the geometrical parameters vary. Therefore, the channel length was fixed to investigate the effect of different geometries of the microchannels on the extraction efficiency at the same residence time. A four-way junction was made by a 3D-printer and was connected to the multiple-ring microchannel through one of its ways. Two ways of this junction with the lengths of 2 cm were used for injecting aqueous and organic phases into the microchannel. The third one was utilized as the pressure transducer connection. Seven multiple-ring microchannels with different geometries were employed in the experiments. As an example, the two multiple-ring microchannels are illustrated in Fig. 2.

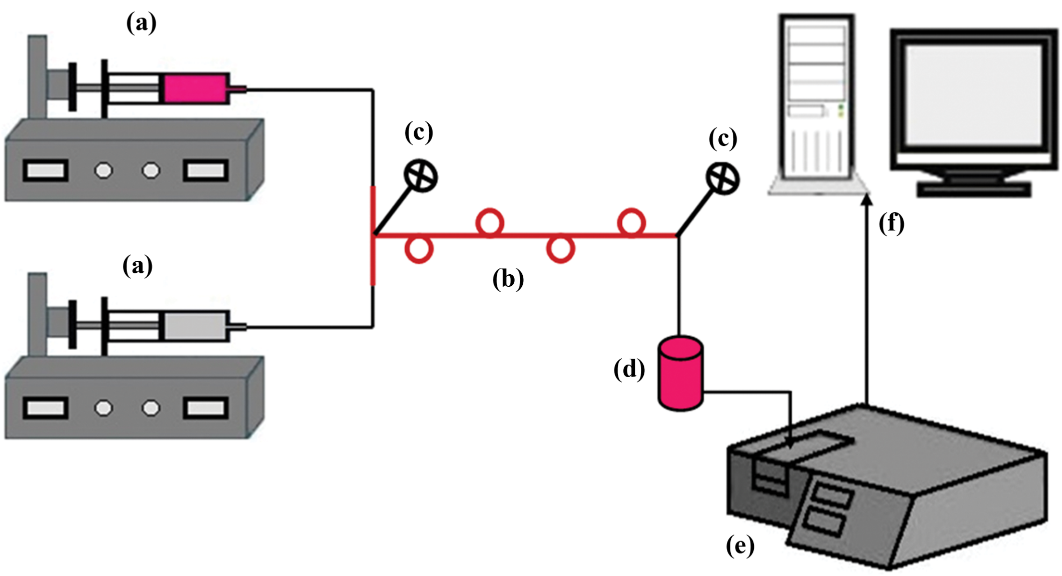

Fig. 1. Schematic layout of the experimental setup: (a) Syringe pumps, (b) multiple-ring microchannel, (c) pressure transducer, (d) sample, (e) spectrophotometer, (f) computer.

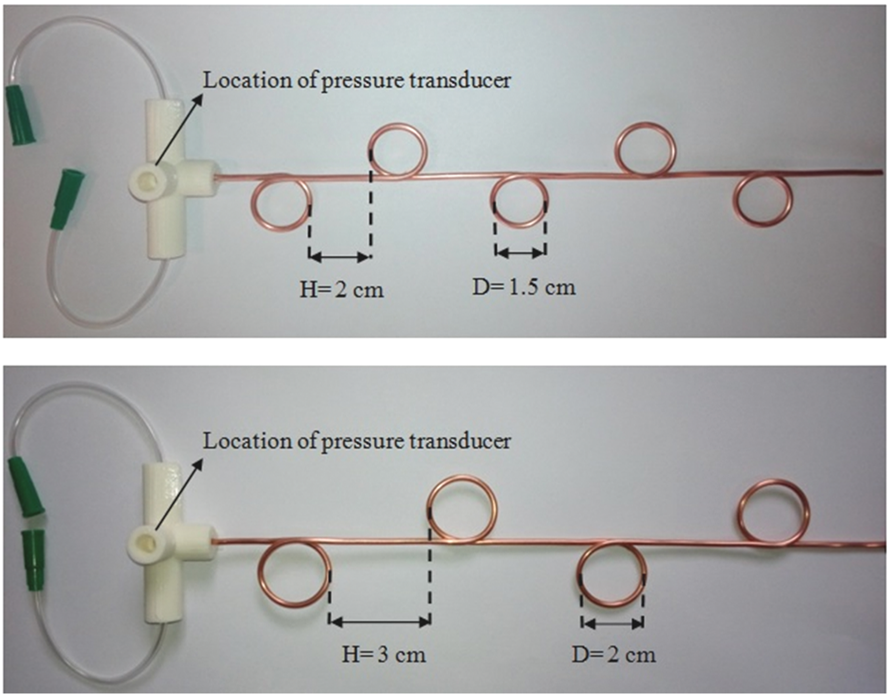

Fig. 2. Multiple-ring microchannels.

In this study, the simultaneous effects of diameter and number of rings as well as the effect of distance between rings on the mass transfer performance were investigated. The dimensionless geometrical parameters of multiple-ring microchannels including rings characteristic (δ) and distance characteristic (β) were defined as follows:

$$\delta=\frac{D}{NL} \tag{1}$$

$$\beta=\frac{H}{L} \tag{2}$$

In which, D, N, H, and L are the rings diameter, the number of rings, the distance between rings, and the total length of microchannels, respectively. Table 1 represents details of the multiple-ring microchannels utilized in this research.

Two syringe pumps (from FNM Company, Iran) were used for injecting aqueous and organic streams into the microchannels. The pressure drop in the microchannels was measured using a pressure transducer (BD sensor type: DMP 343, Germany) connected to a digital display. A UV spectrophotometer (UVmini1240, Shimadzu, Japan) was utilized to determine Alizarin Red S concentration in the aqueous phase.

Table 1. Details of the employed multiple-ring microchannels

Case number	D (cm)	N	H (cm)	δ	β
1	1	6	3	0.003	0.06
2	1.5	5	3	0.006	0.06
3	2	4	3	0.01	0.06
4	2.5	3	3	0.017	0.06
5	1.5	5	2	0.006	0.04
6	1.5	5	1	0.006	0.02
7	1.5	5	0	0.006	0

3. Experimental Procedure

Alizarin Red S was dissolved in deionized water, with the concentration of 1,000 ppm, to prepare the aqueous phase. To extract Alizarin Red S from the aqueous phase, the organic phase contained 0.3 vol% of extractant (Aliquat 336) in diluent (1-octanol) was used. All experiments were at ambient temperature. Two phases were pumped with an equal flow rate into the microchannels by the syringe pumps. Reynolds number values varied in the range of 15 to 180. Alizarin Red S concentration in the outlet aqueous phase of the microchannels was measured by spectrophotometry at a maximum wavelength of 517 nm. To ensure the reproducibility and accuracy of the results, each experiment was repeated three times.

THEORETICAL CONSIDERATIONS

In this study, the extraction of Alizarin Red S was performed based on reactive extraction. A dye-extractant complex is formed at the interface of the two phases. The reaction mechanism between dye and extractant can be described by the following equation [19]:

$$(C_{14}H_7NaO_7S)_{aq}+(C_{25}H_{54}ClN)_{org} \leftrightarrow [(C_{14}H_7O_7S)^-(C_{25}H_{54}N)^+]_{org}+(Na^+Cl^-)_{aq} \tag{3}$$

Reynolds number for the aqueous and organic phases is calculated by the following equations [20]:

$$Re=\frac{\rho_m U_m d}{\mu_m} \tag{4}$$

$$\rho_m = \left(\frac{x_{aq}}{\rho_{aq}} + \frac{1-x_{aq}}{\rho_{org}}\right)^{-1} \tag{5}$$

$$x_{aq} = \frac{Q_{aq}}{Q_{aq}+Q_{org}} \tag{6}$$

$$U_m = \frac{Q_{aq}+Q_{org}}{A} \tag{7}$$

$$\mu_m = \left(\frac{x_{aq}}{\mu_{aq}} + \frac{1-x_{aq}}{\mu_{org}}\right)^{-1} \tag{8}$$

where ρ_m is two-phase mixture density, U_m is two-phase mixture superficial velocity, d is inner diameter of microchannels, μ_m is two-phase mixture viscosity, x_{aq} is volume fraction of aqueous phase, A is the cross-sectional area of the microchannels. Q_{aq} and Q_{org} are flow rates of aqueous and organic phases, respectively.

The mass transfer rate between two-phase is evaluated by the volumetric mass transfer coefficient (k_La). This parameter can be calculated by experimental results as follows [21]:

$$k_La = \frac{1}{t_m}\ln\left(\frac{C_{aq,\,in}-C^*_{aq}}{C_{aq,\,out}-C^*_{aq}}\right) \tag{9}$$

where $C_{aq,\,in}$ and $C_{aq,\,out}$ are the aqueous phase Alizarin Red S concentrations at the microchannel's inlet and outlet, respectively. C^*_{aq} is the equilibrium Alizarin concentration in the aqueous phase. Moreover, t_m is two-phase mixture residence time, which can be defined as follows [21]:

$$t_m = \frac{V}{Q_{org}+Q_{aq}} \tag{10}$$

In which, V is the volume of mixing channel.

The extraction efficiency (E) is the ratio of transferred Alizarin to the maximum transferable Alizarin that is defined as follows [21]:

$$E = \frac{C_{aq,\,in}-C_{aq,\,out}}{C_{aq,\,in}-C^*_{aq}} \tag{11}$$

Simultaneous effects of the extraction efficiency and the pressure drop on the multiple-ring microchannels performance were analyzed by the performance ratio criterion. This criterion can be calculated based on the friction factor and the extraction efficiency as follows [22]:

$$\eta = (E/E_0)/(f/f_0)^{1/3} \tag{12}$$

$$f = \frac{2\Delta P}{(L/d)\rho_m U_m^2} \tag{13}$$

where, f and E are friction factor and extraction efficiency for the multiple-ring microchannels, respectively; f_0 and E_0 are friction factor and extraction efficiency for the plain microchannel, respectively. In Eq. (13), L and ΔP are microchannel length and pressure drop through the microchannels, respectively.

MODELING STUDY

1. Artificial Neural Network and Adaptive Neuro-fuzzy Inference System Description

Artificial neural network is a modeling tool that can estimate complex multivariable functions. Optimum values of the ANN parameters including weights (W) and biases (b) are determined by the training process [23-26]. The final output of the ANN can be determined by the following equation [27-29]:

$$Y = F_a\left\{\sum_{j=1}^{r} W_{kj}\left[F_b\left(\sum_{i=1}^{m} W_{ji}X_i + b_j\right)\right] + b_k\right\} \tag{14}$$

where, Y, r, m, and X are the final ANN output, number of hidden neurons, number of input variables, and network inputs, respectively. F is the transfer function for obtaining the normalized output values.

In the present study, purelin function was considered for the output layer. The performance of sigmoid functions (logsig and tansig) in the hidden layer was evaluated. The developed ANN model for predicting the performance ratio of multiple-ring microchannels has three input variables, including distance characteristic, ring characteristic, and Reynolds number. Since the input and output variables of the ANN have different size ranges, all input data were normalized between (−1) and (1). All input data were divided into two groups including training and testing data. Three-quarters of the input data were selected for developing the ANN (training data)

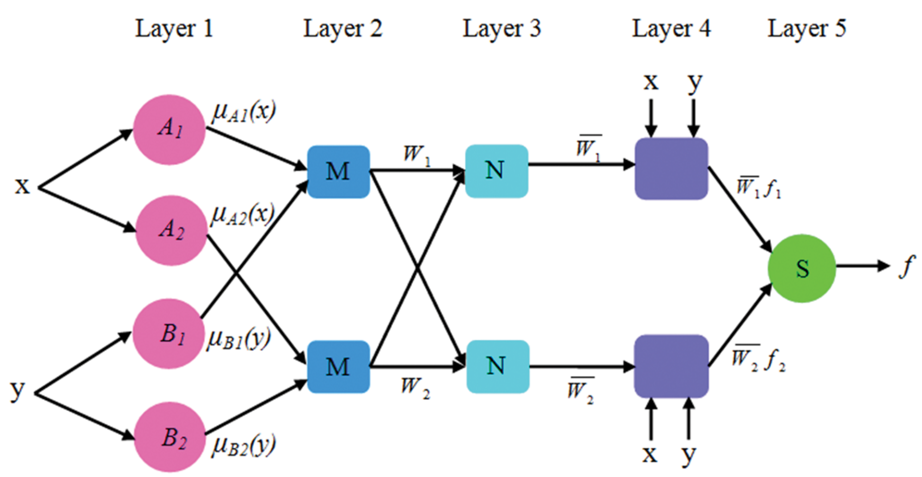

Fig. 3. Diagram of two-input Sugeno fuzzy model with two fuzzy rules.

and a quarter of them were chosen for evaluating the model validity (testing data).

ANFIS uses learning capability of the neural network and reasoning ability of the fuzzy inference system. The parameters of fuzzy inference system including membership functions (MFs) and fuzzy rules can be specified using the neural network [30-34]. The diagram of Sugeno fuzzy model with two fuzzy rules is demonstrated in Fig. 3. As seen, the ANFIS structure was formed from five layers.

In which, A_i and B_i are membership functions. μ_{Ai} (x) and μ_{Bi} (y) are membership grade of x in A_i set and membership grade of y in B_i set, respectively; w_i and $\overline{w}_i$ are weight and normalized weight of the i-th rule, respectively.

In this work, the ANFIS structure was created by the grid partition method. The network was trained based on the hybrid-learning algorithm. The details of modeling process such as input-output variables, data division to the training and testing data set, and data normalization are the same with the ANN modeling procedure.

2. Genetic Algorithm Description

Genetic algorithm, an optimization technique, starts the optimization process with an initial random solution population (chromosomes) and evolves with sequential generations to find the optimal solution. Evaluating objective function, selecting parent chromosomes, and generating new population of chromosomes are the main parts of the genetic algorithm approach. The new chromosomes are generated by genetic operators such as mutation and crossover [35]. The genetic algorithm employs a multi-directional search by retaining a set of potential solutions. The population of chromosomes is changed by reproducing appropriate solutions and eliminating inappropriate solutions at each generation. In this regard, the genetic algorithm utilizes the probabilistic transition rules to find desirable results through the search space. The optimization procedure stops when the algorithm obtains optimum results.

RESULTS AND DISCUSSION

1. Mass Transfer Characteristics

To determine the multiple-ring microchannel with the best performance, evaluating the mass transfer characteristics is necessary. The mass transfer coefficient and the extraction efficiency are proper criteria to evaluate the mass transfer performance. Reynolds number of the fluid flow and geometry of the micromixers are very important parameters. Hence, five Reynolds numbers and seven geometries of the microchannels were examined in the experiments to analyze the extraction performance.

1-1. Mass Transfer Coefficient

Simultaneous effects of the rings diameter and the number of rings on the mass transfer coefficient are shown in Fig. 4(a). It is clear that the mass transfer coefficient increases with increase in Reynolds number, because at high Reynolds numbers, surface renewal velocity and disturbance intensity in the interface of phases increase, so the mass transfer rate between aqueous and organic phases improves.

Fig. 4(a) reveals that the mass transfer coefficient in the multiple-ring microchannels is higher compared with the plain microchannel. It is because of the circular path of the rings that leads to

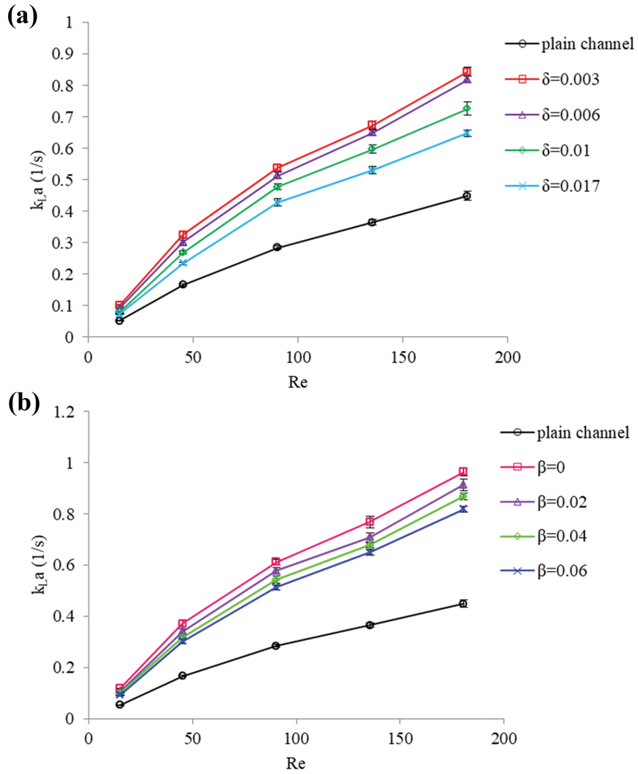

Fig. 4. Effect of (a) δ and (b) β on the mass transfer coefficient.

fluid rotation and centrifugal force. Accordingly, the mixing performance and the mass transfer coefficient are improved by folding and stretching of the fluids interface. Clearly, the role of the multiple-ring microchannel in enhancing the mass transfer coefficient at high Reynolds numbers is more effective than that at low Reynolds numbers. Thus, the centrifugal force induced by the fluid rotation at high Reynolds numbers is more intensive than that at low Reynolds numbers. The values of mass transfer coefficient at δ=0.003 are 1.8-2 times higher than those in the plain microchannel. According to Fig. 4(a), a decrease in δ enhances the mass transfer coefficient. In fact, at a fixed total length of the microchannels, reduction in δ indicates a decrease in the rings diameter and an increase in the number of rings. Although the decrease in the rings diameter leads to a short rotational flow path in the rings, an increase in the number of rings causes the improvement of two-phase mixing performance.

To achieve a higher mass transfer coefficient at a fixed δ, the distance between rings was varied. The effect of distance characteristic (β) on the mass transfer coefficient at different Reynolds numbers is shown in Fig. 4(b): The mass transfer coefficient improves when β decreases. Reduction in β at a fixed δ means that the rings become closer to the microchannel junction. Therefore, arranging rings close to the junction is more effective than distributing them through the mixing channel evenly. For example, as β decreases from 0.06 to 0, the mass transfer coefficient improves 17.7-28.2% at different Reynolds numbers. This can be explained by the fact that a decrease in the distance between rings leads to a higher interface disturbance of two-phase and more efficient mixing. So, two-phase mixing in the array of rings close to the junction happens faster than that in

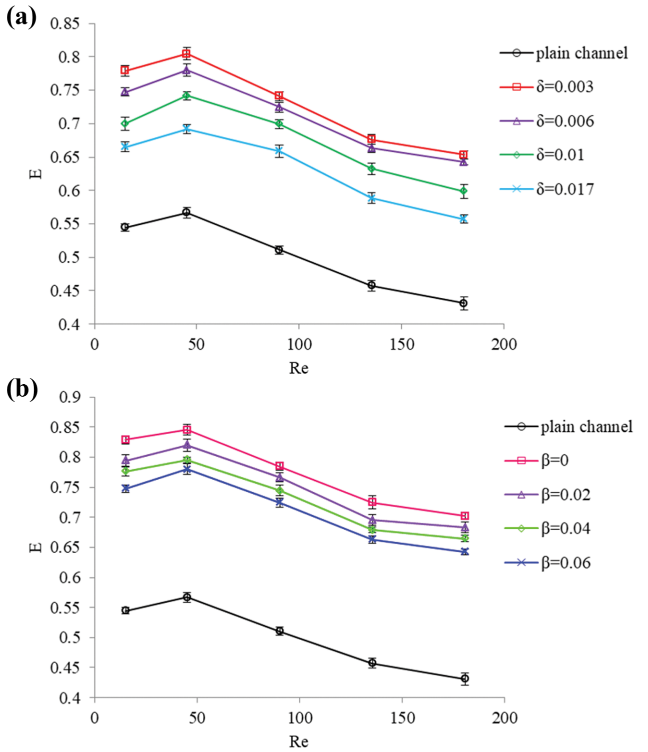

Fig. 5. Extraction efficiency in the multiple-ring microchannels as a function of (a) δ and (b) β.

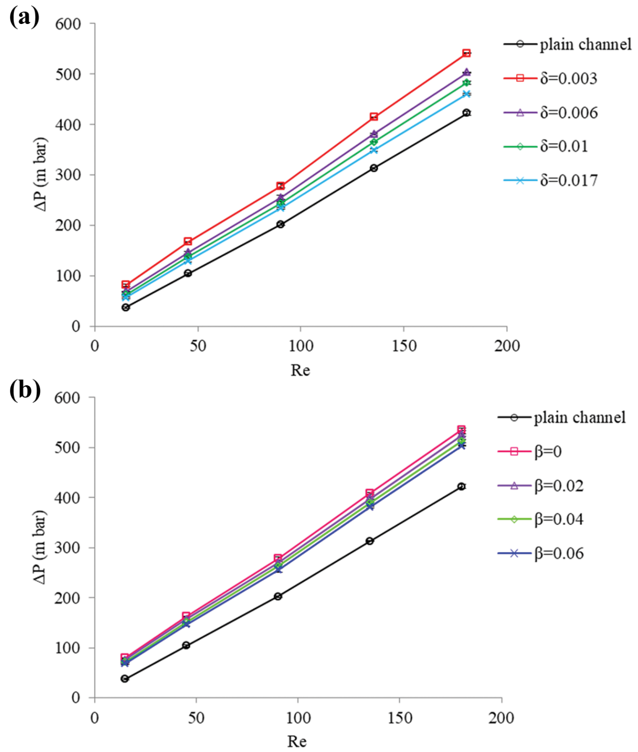

Fig. 6. Effect of (a) δ and (b) β on the pressure drop.

the evenly distributed arrangement. This feature reduces the mass transfer resistance and consequently enhances the mass transfer coefficient in the microchannel.

1-2. Extraction Efficiency

Fig. 5(a) illustrates the extraction efficiency of Alizarin versus Reynolds number at different values of δ. For all microchannels, the extraction efficiency does not show a constant trend with the change in Reynolds number. As Reynolds number increases, the extraction efficiency first increases and then decreases. This is due to the dependency of extraction efficiency on the mass transfer coefficient and the fluid residence time in microchannels [20,22]. The extraction efficiency has a direct relationship with these parameters. As mentioned, the mass transfer coefficient improves with an increase in Reynolds number. In contrast, the fluid residence time is reduced by increasing Reynolds number. Therefore, it is clear that at low Reynolds numbers, enhancement in the mass transfer coefficient is the dominant effect, but at high Reynolds numbers a reduction in the fluid residence time plays the dominant role.

As indicated in Fig. 5(a), the extraction efficiency has improved in the multiple-ring microchannels compared with the plain one. This is because of the higher mass transfer coefficient in the multiple-ring microchannels in comparison with the plain one at the same residence time that results in higher extraction efficiency. As shown in Fig. 5(a), the extraction efficiency has increased at low values of δ. The results show that the decrease in δ from 0.017 to 0.003 enhances the extraction efficiency in the range of 12.5-17.3%. The reason is that with decrease in δ, the fluid residence time does not change because the total volume of the microchannels is constant. Moreover, as mentioned, the decrease in δ leads to improvement in the mass transfer coefficient. Therefore, the extraction is intensified by decreasing the value of δ.

Fig. 5(b) indicates the extraction efficiency in the microchannels as a function of β. As can be seen, the extraction efficiency has an increasing trend with decrease in the value of β. Variation in the value of β from 0.06 to 0 leads to an improvement in extraction efficiency in the range of 8.3-10.9% at different Reynolds numbers. It can be explained that the decrease in β has no effect on the residence time and only increases the mass transfer coefficient. Hence, the positive effect of decreasing β leads to an enhancement in extraction efficiency. The maximum extraction efficiency was achieved in β=0 with 49.1-62.9% enhancement compared with the plain microchannel.

2. Evaluation of Pressure Drop

Modifying the geometry of microchannels with the aim of improvement in the mass transfer performance usually shows an adverse influence on the pressure drop. Therefore, it is essential to evaluate the pressure drop in the microchannels which is directly related to the required energy for moving fluids through the mixing channel. The pressure drop in the multiple-ring microchannels with different values of δ is depicted in Fig. 6(a). It can be noted that in all microchannels, the pressure drop increases as Reynolds number increases. In fact, an increase in Reynolds number leads to an increase in the fluid velocity that consequently increases the pressure drop. In addition, Fig. 6(a) shows that the pressure drop in the multiple-ring microchannels is higher than that in the plain one because of the rotational path of fluid flow through these microchannels. The results demonstrate that the pressure drop increases with a decrease in the value of δ. With a reduction in δ, the number of rings and accordingly fluid rotation in the mixing channel increase. The pressure drop values in the multiple-ring microchannel with δ=0.003 are 1.3-2.2 times higher than those in the plain one at different Reynolds numbers. Fig. 6(b) reveals the pressure drop in the multiple-ring microchannels with various values of β. It can be seen from Fig. 6(b) that the reduction of β has a slight effect on the pressure drop. With a decrease in β, the number of rings does not change and only the rings get close to each other so the pressure drop increases slightly.

3. Performance Ratio

Although multiple-ring microchannels have an efficient influence on the mass transfer characteristics, they lead to a further pressure drop. The performance ratio is a useful criterion to judge the performance of the multiple-ring microchannels. The simultaneous analysis of the extraction efficiency and the pressure drop using the performance ratio can help the optimal design of microchannels. The performance ratio of the studied microchannels with different values of δ is indicated in Fig. 7(a). Since the plain channel is the reference layout for comparing the multiple-ring microchannels, its performance ratio value is equal to 1 (based on Eq. (13)). As shown in Fig. 7(a), performance ratio values in multiple ring microchannels are higher than 1. This proves that the performance of liquid-liquid extraction has improved in the multiple-ring microchannels. The results show that a reduction in δ to the value of 0.006 enhances the performance ratio. The performance ratio values in the microchannel with δ=0.006 are in the range of 1.12-1.41 at different Reynolds numbers. As the value of δ decreases from 0.006 to 0.003, the performance ratio also decreases. This is because of the further increase in the pressure drop compared with the extraction efficiency at low values of δ.

The effect of β on the performance ratio is revealed in Fig. 7(b): A decrease in the value of β leads to an enhancement in the performance ratio. As mentioned, the change in β has a slight effect on the pressure drop. Thus, with the reduction of β, the influence of extraction efficiency is dominant compared with that of pressure drop, which results in the improvement of performance ratio. The highest performance ratio values in the range of 1.18-1.5 were obtained in the multiple-ring microchannel with β=0.

4. ANN Modeling Results

Various structures of the ANN were evaluated by the root mean square error (RMSE), mean relative error (MRE), and determination coefficient (R^2) based on the following equations:

$$\mathrm{RMSE}=\sqrt{\frac{1}{n}\sum_{i=1}^{n}(t_i-y_i)^2} \tag{15}$$

$$\mathrm{MRE}\ (\%)=\frac{100}{n}\sum_{i=1}^{n}\left(\frac{|t_i-y_i|}{t_i}\right) \tag{16}$$

$$R^2=1-\frac{\sum_{i=1}^{n}(y_i-t_i)^2}{\sum_{i=1}^{n}(t_i-t_a)^2} \tag{17}$$

where, n, t, y, and t_a are the number of data points, target data (actual data), predicted values, and average of target data, respectively.

Error values of different ANN models with tansig and logsig functions in the hidden layer were examined. RMSE values of these ANN structures are illustrated in Fig. 8. According to Fig. 8, the ANN with logsig transfer function and six hidden neurons has the smallest RMSE value. In fact, the optimum number of neurons in the hidden layer was determined by trial and error. An increase in the number of hidden neurons may lead to the over-fitting prob-

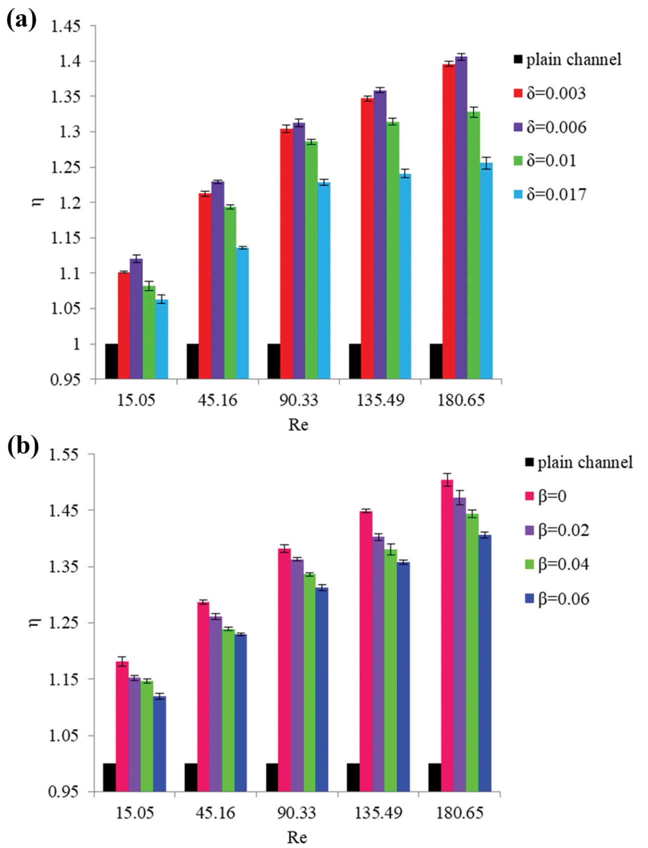

Fig. 7. Performance ratio of the studied microchannels with different values of (a) δ and (b) β.

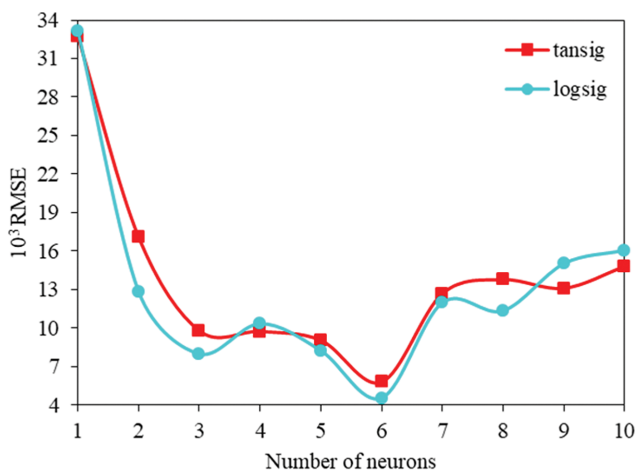

Fig. 8. RMSE values of different ANN structures.

Table 2. RMSE, MRE and R^2 values for ANNs with different numbers of hidden neurons

Number of neurons	RMSE	MRE (%)	R^2
1	0.03317	2.088	0.9168
2	0.01284	0.802	0.9875
3	0.00797	0.476	0.9952
4	0.01033	0.641	0.9919
5	0.00823	0.367	0.9949
6	0.00454	0.230	0.9984
7	0.01197	0.597	0.9892
8	0.01134	0.559	0.9903
9	0.01501	0.633	0.9830
10	0.01606	0.720	0.9805

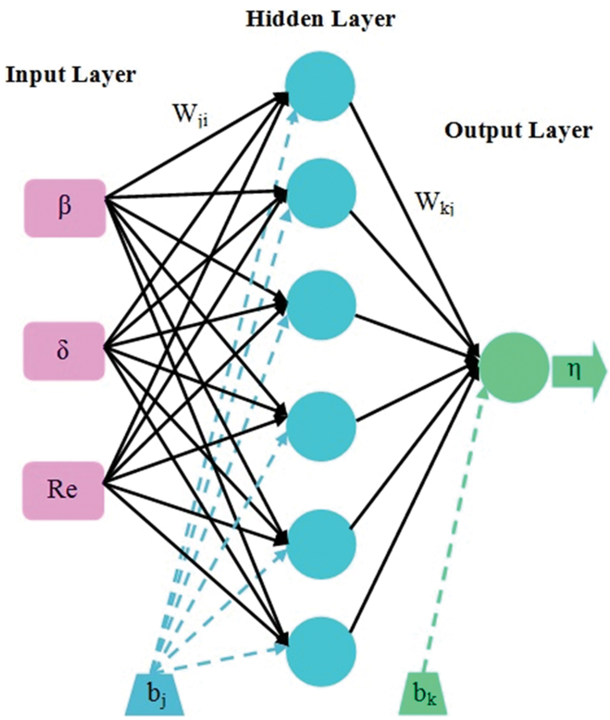

Fig. 9. Structure of the developed ANN model (3-6-1).

lem. Hence, the training process was started with one hidden neuron, then the number of hidden neurons was increased to find the optimum error value.

The values of RMSE, MRE, and R^2 for ANNs with logsig transfer function and various numbers of hidden neurons are listed in Table 2. According to Table 2, the ANN with six hidden neurons is selected as the optimal structure that has RMSE, MRE, and R^2 of 0.00454, 0.230, and 0.9984, respectively.

Fig. 9 reveals the structure of the developed ANN model (3-6-1) in this work. Weights and biases of the proposed ANN model (3-6-1) are given in Table 3. The performance ratio of the multiple-ring microchannels can be calculated by putting the presented weights and biases in Eq. (14).

To study the precision of the ANN model in estimating the performance ratio, the actual data were compared with the predicted

Table 3. Weights and biases of the proposed ANN model for prediction of η

Neuron	W_{ji}			b_j	b_k=−2.4947
	β	δ	Re		W_{kj}
1	−1.1165	4.6990	0.2356	6.5475	2.2476
2	−0.0382	5.8002	1.8767	1.6337	0.3902
3	1.7517	−0.4249	−1.5831	−3.1300	0.6061
4	−0.2408	−1.9601	0.4369	−2.0648	3.1619
5	0.1533	0.5914	−3.4880	−3.1495	−1.6034
6	2.7965	−4.0539	2.9087	4.9251	−0.3544

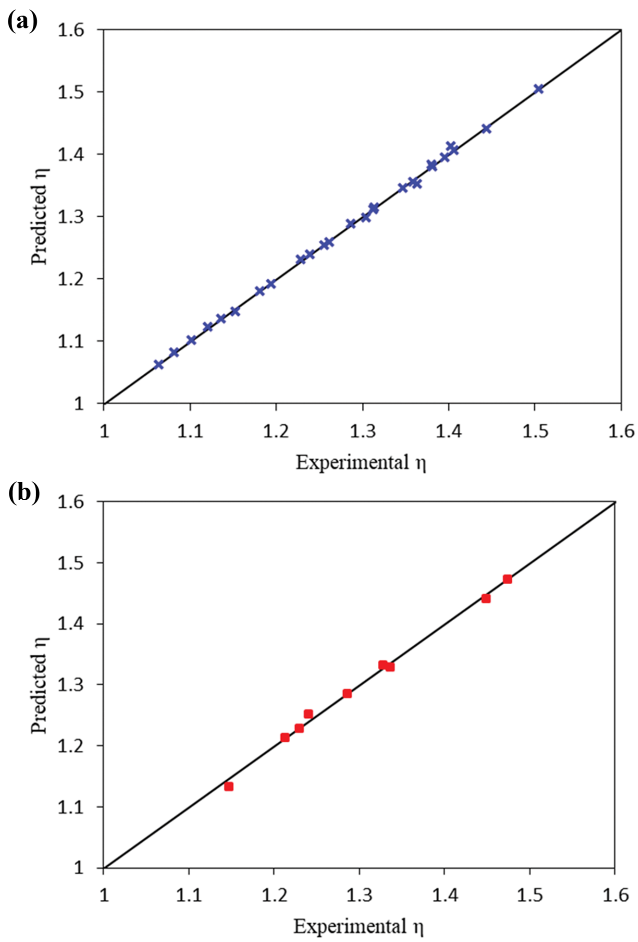

Fig. 10. A comparison between predicted performance ratio values by the ANN and experimental results: (a) Training data and (b) testing data.

values. Fig. 10 illustrates predicted values by the ANN versus experimental results for training data (Fig. 10(a)) and testing data (Fig. 10(b)). An excellent correlation between predicted values and experimental results is shown in Fig. 10. Moreover, the high accuracy of testing data proves the model validity.

5. ANFIS Modeling Results

The ANFIS modeling approach was employed to estimate the performance ratio of multiple-ring microchannels. To find the model structure with minimum error, common membership functions

Table 4. RMSE values for different ANFIS structures

Structure number	Number of MFs	Number of fuzzy rules	MF type					
			Triangular	Trapezoidal	Generalized	Gaussian bell	Combination gaussian	Π-shaped
1	2/2/2	8	0.01204	0.00796	0.00976	0.00908	0.00996	0.00767
2	3/2/2	12	0.01006	0.00740	0.00856	0.00869	0.00835	0.00776
3	2/3/2	12	0.01368	0.02517	0.04438	0.05957	0.04768	0.08530
4	2/2/3	12	0.01945	0.01300	0.02890	0.01964	0.05904	0.03509
5	3/3/2	18	0.02246	0.02634	0.05016	0.04854	0.05730	0.06473
6	3/2/3	18	0.04841	0.04505	0.03273	0.03853	0.05139	0.03301
7	2/3/3	18	0.02031	0.13309	0.02505	0.05927	0.14266	0.21239
8	3/3/3	27	0.07197	0.07176	0.05618	0.08122	0.07557	0.10012
9	4/2/2	16	0.01882	0.04330	0.03646	0.01797	0.01844	0.04876
10	2/4/2	16	0.01366	0.02518	0.01349	0.01106	0.01623	0.02518
11	2/2/4	16	0.05429	0.09651	0.03874	0.03010	0.09919	0.11474
12	4/4/2	32	0.00827	0.06271	0.03205	0.01951	0.06038	0.06946
13	4/2/4	32	0.35296	0.35834	0.25649	0.27568	0.37541	0.37758
14	2/4/4	32	0.30777	0.19287	0.11929	0.27181	0.18451	0.20045

including triangular, gaussian, trapezoidal, combination-gaussian, generalized bell, and Π-shaped with different structures were investigated. In addition, for each membership function, the number of membership functions of input variables was also examined. The number of fuzzy rules can be obtained by multiplying the number of membership functions of input variables. Therefore, Table 4 reports error (RMSE) values related to various numbers of membership functions and fuzzy rules for different types of membership functions. The results reveal that a large number of membership functions and fuzzy rules can lead to the complexity of the network structure and reduction of the model accuracy. Therefore, up to 32 fuzzy rules were used in the ANFIS structure. The lowest RMSE value of 0.0074 was obtained by the structure of 3, 2, and 2 trapezoidal membership functions for β, η, and Re, respectively. The trapezoidal membership function is defined by the following equation:

$$\mu_{Ai}(x)=\begin{cases} 0 & x\le a \\ \dfrac{x-a}{b-a} & a\le x\le b \\ 1 & b\le x\le c \\ \dfrac{d-x}{d-c} & c\le x\le d \\ 0 & d\le x \end{cases} \tag{18}$$

where, a, b, c, and d are the trapezoidal function parameters.

An evaluation of the model accuracy for predicting the performance ratio is shown in Fig. 11. An excellent agreement between the estimated and actual values is observed in Fig. 11. The high precision of the ANFIS model for estimating the testing data set confirms the model validity.

6. Proposing Empirical Correlation

In this research, we tried to develop a novel empirical correlation for the performance ratio as a function of Reynolds number and geometrical parameters of the multiple-ring microchannels. In this regard, the genetic algorithm technique was used because of its superiority in finding the optimum response compared with the traditional methods such as the least square analysis. Experimen-

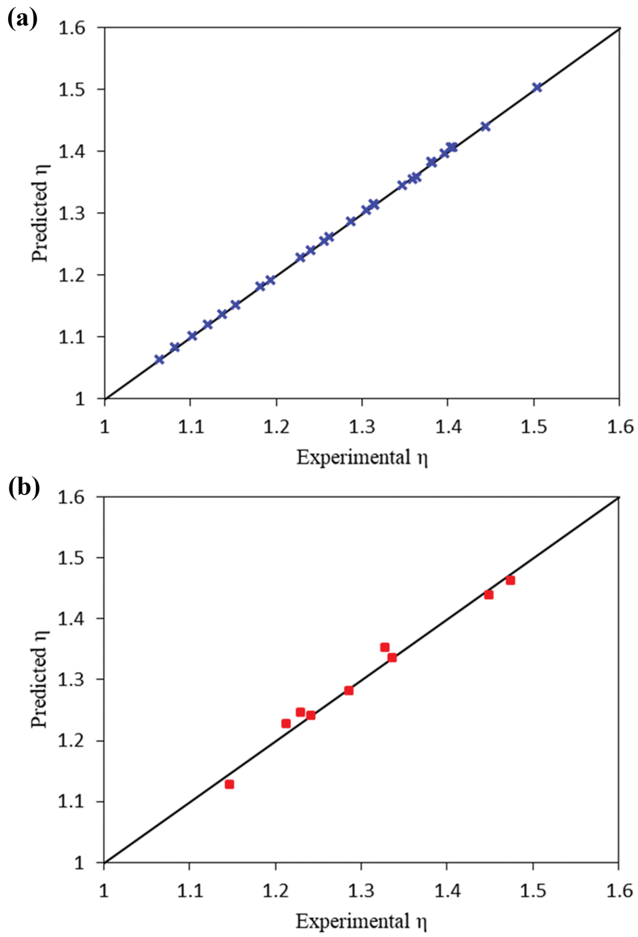

Fig. 11. A comparison between predicted performance ratio values by the ANFIS and experimental results: (a) Training data and (b) testing data.

tal data of the performance ratio for seven multiple-ring microchannels were utilized to develop an empirical correlation. Therefore, an equation was assumed in the form of power-law correlation as follows:

$$\eta = c_1\beta^{c_2}\delta^{c_3} + \mathrm{Re}^{c_4} \tag{19}$$

where, c_i is the constant of the equation.

The fitness function was defined based on RMSE between experimental data and predicted values as follows:

$$E(c_1, c_2, c_3, c_4) = \sqrt{\frac{1}{n}\sum_{i=1}^{n}(\eta_i^{Exp} - \eta_i^{Pred})^2} \tag{20}$$

where, n is the number of experimental data points and superscripts of 'Exp' and 'Pred' refer to actual and predicted values, respectively. The genetic algorithm technique was used to obtain the equation constants with the aim of minimizing the fitness function. The details of the genetic algorithm approach were the number of chromosomes for initial random solution population=150, the crossover fraction=0.8, and the number of elite children=2. The optimization process was stopped after 600 generations and the following equation was obtained:

$$\eta = -7.5728\beta^{0.6714}\delta^{0.4471} + \mathrm{Re}^{0.0761} \tag{21}$$

The deviation of the proposed equation was analyzed based on RMSE and MRE. MRE value of the proposed correlation is 1.558%. The predicted values of the performance ratio versus the experimental results are illustrated in Fig. 12. The results represent an acceptable agreement between predicted values by Eq. (21) and experimental results.

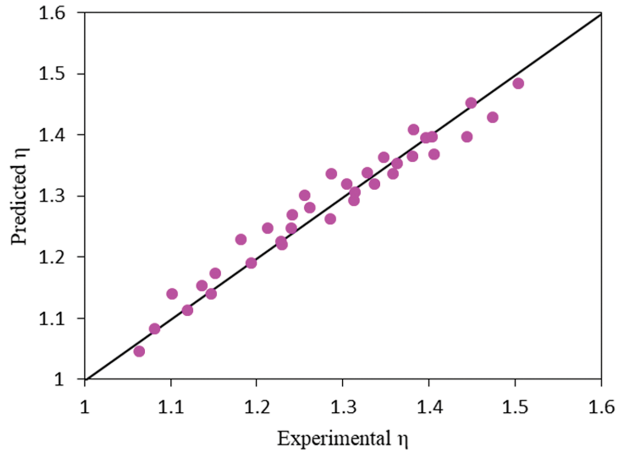

Fig. 12. A comparison between estimated performance ratio values by the empirical correlation and experimental results.

7. Comparison between ANN, ANFIS, and GA Based Correlation

The accuracy of the ANN, ANFIS, and GA based correlation for predicting the performance ratio was evaluated. The values of RMSE and MRE for these approaches are presented in Table 5. The results of Table 5 illustrate that ANN is the most accurate model for estimating the performance ratio. The higher accuracy of the ANN compared with the ANFIS and the GA based correlation is confirmed by error values of the testing data, which were not utilized in the training process. MRE values of the testing data set are 0.397% and 0.888% for ANN and ANFIS models, respectively. In addition, the MRE value of the empirical correlation is 1.558%. Although the error value of the GA based correlation is higher than that of the ANN and ANFIS, it is evident that using the empirical equation for estimating the performance ratio is more practical than other models.

Table 5. Deviations of ANN, ANFIS, and empirical correlation for prediction of η

Model	Stage	RMSE	MRE (%)
ANN	Training	0.00344	0.172
	Testing	0.00677	0.397
	Overall	0.00454	0.230
ANFIS	Training	0.00202	0.097
	Testing	0.01418	0.888
	Overall	0.00740	0.301
GA based correlation		0.02470	1.558

The most important advantage of this work is the potential of the employed models to predict the better performance of multiple-ring microchannels. A higher performance ratio can be obtained by changing the input parameters. Different values of input parameters (D, N, H, and Re) can be tested using the prediction models to estimate a higher performance ratio. In fact, better performance can be achieved by trying various input parameters in the developed models instead of performing experiments.

8. Comparison with other Studies

The volumetric mass transfer coefficient values in this work were compared with those in other types of microchannels in Table 6. The lowest k_La values were obtained by the T-micromixer and vertical microchannel. This is because of the plain mixing channel

Table 6. Volumetric mass transfer coefficient values in the current work and other types of microchannels

Type of microchannel	Channel diameter (hydraulic diameter) (mm)	System	k_La (1/s)	Reference
Multiple-ring microchannel	0.8	Water+Alizarin+1-octanol	0.072-0.964	Present study
T-micromixer	0.25	Water+succinic acid+n-butanol	0.013-0.079	[6]
Vertical microchannel	0.8	Water+succinic acid+n-butanol	0.012-0.082	[8]
Split and recombine microchannel	0.25	Water+succinic acid+n-butanol	0.022-0.16	[6]
Serpentine microchannel	(0.3-0.7)	Samarium (III)+hydrochloric acid+ 2-ethylhexyl phosphonic acid	0.07-1.14	[36]

Table 7. A comparison between error values of artificial intelligence in this study and other extraction processes

Process	Technique	RMSE	MRE (%)	Reference
Alizarin extraction in multiple-ring microchannels	Modeling of η by ANN (as the best model)	0.0045	0.230	Present study
Solvent extraction of lanthanum from acidic nitrate	Modeling of extraction percentage by ANN	0.005	-	[37]
Dye microextraction based on ultrasound-assisted	Prediction of extraction percentage by ANN	0.0034	-	[38]
Aromatics extraction in rotating disc contactor	Prediction of extraction yield by ANN	-	0.191	[39]
Quercetin extraction via supercritical CO_2	Modeling of Quercetin recovery by ANFIS	0.831	-	[40]
Extraction of Glycyrrhizic acid using supercritical CO_2	Modeling of extraction recovery by ANFIS	0.412	-	[41]

of these micromixers. Table 6 shows that k_La values of the present work are higher than those of the split and recombine microchannel. In addition, k_La values obtained in the present study are in agreement with those in the serpentine microchannel, considering that the hydraulic diameter of the employed serpentine microchannel is lower than the diameter of multiple-ring microchannels. In fact, a decrease in the channel diameter enhances the volumetric mass transfer coefficient. Hence, this comparison demonstrates that multiple-ring microchannels are attractive tools for intensifying liquid-liquid mass transfer.

Table 7 reports the error values of artificial intelligence in this study and other extraction processes. The results of Table 7 show that the error values presented by ANFIS models are higher than those by ANN approaches. The present study is consistent with works done by Acharya and Mishra [37] and Dil et al. [38] because the error values in three studies are close to each other. Moreover, the error value of ANN in the work done by Mehrkesh et al. [39] is slightly lower than that in the present study. Therefore, the prediction accuracy in the present study is appropriate for modeling liquid-liquid extraction in multiple-ring microchannels.

CONCLUSIONS

The liquid-liquid mass transfer performance of multiple-ring microchannels was investigated at various Reynolds numbers between 15 and 180. The effects of Reynolds number as well as geometrical parameters including the ring characteristic (δ) and the distance characteristic (β) on the mass transfer performance were evaluated. The results showed that at lower values of δ and β, the extraction efficiency of the multiple-ring microchannels improved between 49.1 and 62.9% compared with that of the plain microchannel. Although the mass transfer is intensified in the multiple-ring microchannels, a further pressure drop was also created in these channels. The pressure drop values of multiple-ring microchannels at δ=0.003 and β=0.06 were 1.3-2.2 times higher than those of the plain one at various Reynolds numbers. Therefore, the performance ratio was defined as a function of friction factor and extraction efficiency to evaluate the multiple-ring microchannels performance. The performance ratio values of more than one indicate the enhancement of mass transfer performance in the multiple-ring microchannel compared with the plain microchannel. The results show that the performance ratio increased with a reduction in β. However, its values had an ascending-descending trend with a decrease in δ. The highest performance ratio values in the range between 1.18 and 1.50 were achieved at δ=0.006 and β=0.

Artificial intelligence approaches, including ANN and ANFIS, were employed to model the performance ratio of multiple-ring microchannels. The results revealed an excellent agreement between the predicted values and the experimental results. Error analysis for the testing data set showed that MRE values for ANN and ANFIS models are 0.397% and 0.888%, respectively. Hence, ANN was found more accurate than ANFIS for estimating the performance ratio. A novel empirical correlation was proposed for predicting the performance ratio as a function of Reynolds number and geometrical parameters. Genetic algorithm technique was used for finding the equation constants. MRE value of 1.558% indicated that predicted values were in an appropriate agreement with experimental results. The accuracy of GA based correlation is lower than the ANN and ANFIS models. Despite the greater accuracy of ANN compared with the empirical correlation, the computational cost of ANN is higher than that of the empirical correlation. Sometimes, using less accurate methods is more efficient due to their low cost. Thus, selecting the appropriate method depends on the required accuracy in each case study.

NOMENCLATURE

A : cross-sectional area of the microchannel [m^2]
A_1 and A_2 : membership function
B_1 and B_2 : membership function
b : bias
C : Alizarin Red S concentration [mg/L]
c_i : constant
D : rings diameter [m]
d : inner diameter of the microchannels [m]
E : extraction efficiency
F : transfer function
f : friction factor

H : distance between rings [m]
k_La : volumetric mass transfer coefficient [1/s]
L : total length of the microchannels [m]
m : number of input variables
N : number of rings
n : number of experimental data points
ΔP : pressure drop [mbar]
Q : volumetric flow rate [m^3/s]
r : number of neurons
Re : Reynolds number
t_a : average of the target data
t_i : target data
t_m : fluid residence time [s]
U_m : two-phase mixture superficial velocity [m/s]
V : volume of the mixing channel [m^3]
W : weight
X : network input
x : volume fraction of phases
Y : final output of the network

Greek Letter
ρ : density [kg/m^3]
μ : dynamic viscosity [Pa s]
η : performance ratio criterion [-]
δ : rings characteristic [-]
β : distance characteristic [-]

Subscripts/Superscript
A : average
aq : aqueous phase
Exp : experimental results
in : inlet
m : two-phase mixture
org : organic phase
out : outlet
Pred : predicted values
* : equilibrium

REFERENCES

1. A. Afzal and K.-Y. Kim, *Chem. Eng. Sci.*, **116**, 263 (2014).
2. Y. S. Huh, S. J. Jeon, E. Z. Lee, H. S. Park and W. H. Hong, *Korean J. Chem. Eng.*, **28**, 633 (2011).
3. M. Mohadesi, B. Aghel, M. H. Khademi and S. Sahraei, *Korean J. Chem. Eng.*, **34**, 1013 (2017).
4. M. Sato and M. Goto, *Sep. Sci. Technol.*, **39**, 3163 (2004).
5. Y. Yamasaki, M. Goto, A. Kariyasaki, S. Morooka, Y. Yamaguchi, M. Miyazaki and H. Maeda, *Korean J. Chem. Eng.*, **26**, 1759 (2010).
6. K. Singh, A. Renjith and K. Shenoy, *Chem. Eng. Process.*, **98**, 95 (2015).
7. A. J. Tušek, I. Anić, Ž. Kurtanjek and B. Zelić, *Korean J. Chem. Eng.*, **32**, 1037 (2015).
8. J. Tang, X. Zhang, W. Cai and F. Wang, *Exp. Therm. Fluid Sci.*, **49**, 185 (2013).
9. F. H. Kakavandi, M. Rahimi, O. Jafari and N. Azimi, *Chem. Eng. Process.*, **107**, 58 (2016).
10. L. Zhang, F. Xie, S. Li, S. Yin, J. Peng and S. Ju, *Green. Process. Synth.*, **4**, 3 (2015).
11. A. Kaewchada, S. Tubslingkra and A. Jaree, *Chem. Eng. Res. Des.*, **117**, 784 (2017).
12. D. Das, S. Duraiswamy, Z. Yi, V. Chan and C. Yang, *Sep. Sci. Technol.*, **50**, 1023 (2015).
13. S. Hossain, M. Ansari and K.-Y. Kim, *Chem. Eng. J.*, **150**, 492 (2009).
14. I. Shah, S. W. Kim, K. Kim, Y. H. Doh and K. H. Choi, *Chem. Eng. J.*, **358**, 691 (2019).
15. A. A. Babaei, A. Khataee, E. Ahmadpour, M. Sheydaei, B. Kakavandi and Z. Alaee, *Korean J. Chem. Eng.*, **33**, 1352 (2016).
16. M. Molashahi and H. Hashemipour, *Korean J. Chem. Eng.*, **29**, 601 (2012).
17. M. S. V. Krishna, K. M. S. Begum and N. Anantharaman, *Powder Technol.*, **307**, 37 (2017).
18. A. Lashkaripour, M. Goharimanesh, A. A. Mehrizi and D. Densmore, *Microelectron. J.*, **78**, 73 (2018).
19. F. H. Kakavandi, M. Rahimi, M. Baniamer and H. R. Mahdavi, *Chem. Pap.*, **71**, 2521 (2017).
20. Y. Zhao, G. Chen and Q. Yuan, *AIChE J.*, **53**, 3042 (2007).
21. D. Tsaoulidis, V. Dore, P. Angeli, N. V. Plechkova and K. R. Seddon, *Chem. Eng. J.*, **227**, 151 (2013).
22. M. Rahimi, S. R. Shabanian and A. A. Alsairafi, *Chem. Eng. Process.*, **48**, 762 (2009).
23. S. R. Moosavi, D. A. Wood, M. A. Ahmadi and A. Choubineh, *Nat. Resour. Res.*, **28**, 1619 (2019).
24. M. A. Ahmadi, M. Ebadi and A. Yazdanpanah, *J. Pet. Sci. Eng.*, **123**, 7 (2014).
25. M. A. Ahmadi, M. Masumi, R. Kharrat and A. H. Mohammadi, *Chem. Eng. Technol.*, **37**, 409 (2014).
26. M. A. Ahmadi, *Math. Probl. Eng.*, **2015**, 1 (2015).
27. M. A. Ahmadi and S. R. Shadizadeh, *Fuel*, **102**, 716 (2012).
28. M. A. Ahmadi, *Fluid Phase Equilib.*, **314**, 46 (2012).
29. M. A. Ahmadi, *J. Pet. Explor. Prod. Technol.*, **1**, 99 (2011).
30. M. A. Ahmadi and A. Ahmadi, *Int. J. Low Carbon Technol.*, **11**, 325 (2016).
31. M.-A. Ahmadi, M. R. Ahmadi, S. M. Hosseini and M. Ebadi, *J. Pet. Sci. Eng.*, **123**, 183 (2014).
32. M.-A. Ahmadi, A. Bahadori and S. R. Shadizadeh, *Fuel*, **139**, 154 (2015).
33. M. A. Ahmadi, M. Ebadi, P. S. Marghmaleki and M. M. Fouladi, *Fuel*, **124**, 241 (2014).
34. M. A. Ahmadi and M. Ebadi, *Fuel*, **117**, 1074 (2014).
35. C. C. Yuen, S. K. Gupta and A. K. Ray, *J. Membr. Sci.*, **176**, 177 (2000).
36. Y. He, J. Pei, C. Srinivasakannan, S. Li, J. Peng, S. Guo, L. Zhang and S. Yin, *Hydrometallurgy*, **179**, 175 (2018).
37. S. Acharya and S. Mishra, *Sep. Sci. Technol.*, **52**, 1660 (2017).
38. E. A. Dil, M. Ghaedi and A. Asfaram, *Ultrason. Sonochem.*, **34**, 27 (2017).
39. A. H. Mehrkesh, S. Hajimirzaee, M. S. Hatamipour and T. Tavakoli, *Chem. Eng. Technol.*, **34**, 459 (2011).
40. S. Ghoreishi, A. Hedayati and S. Mousavi, *J. Supercrit. Fluids*, **112**, 57 (2016).
41. A. Hedayati and S. Ghoreishi, *Chem. Prod. Process. Model.*, **11**, 217 (2016).